A&A 512, A22 (2010)
DOI: 10.1051/0004-6361/200811319
© ESO 2010

Astronomy & Astrophysics

γ Cassiopeiae: an X-ray Be star with personality*

R. Lopes de Oliveira[1], M. A. Smith[2], and C. Motch[3]

[1] Universidade de São Paulo, Instituto de Astronomia, Geofísica e Ciências Atmosféricas, R. do Matão 1226, 05508-090 São Paulo, Brazil
e-mail: rlopes@astro.iag.usp.br
[2] Catholic University of America, 3700 San Martin Drive, Baltimore, MD 21218, USA
[3] Université de Strasbourg, CNRS, UMR 7550, Observatoire Astronomique, 11 rue de l'Université, 67000 Strasbourg, France

Received 10 November 2008 / Accepted 6 January 2010

ABSTRACT

An exciting unsolved problem in the study of high energy processes of early type stars concerns the physical mechanism for producing X-rays near the Be star γ Cassiopeiae. By now we know that this source and several "γ Cas analogs" exhibit an unusual hard thermal X-ray spectrum, compared both to normal massive stars and the non-thermal emission of known Be/X-ray binaries. Also, its light curve is variable on almost all conceivable timescales. In this study we reanalyze a high dispersion spectrum obtained by *Chandra* in 2001 and combine it with the analysis of a new (2004) spectrum and light curve obtained by XMM-*Newton*. We find that both spectra can be fit well with 3–4 optically thin, thermal components consisting of a hot component having a temperature $kT_Q \sim 12$–14 keV, *perhaps* one with a value of ~2.4 keV, and two with well defined values near 0.6 keV and 0.11 keV. We argue that these components arise in discrete (almost monothermal) plasmas. Moreover, they cannot be produced within an integral gas structure or by the cooling of a dominant hot process. Consistent with earlier findings, we also find that the Fe abundance arising from K-shell ions is significantly subsolar and less than the Fe abundance from L-shell ions. We also find novel properties not present in the earlier *Chandra* spectrum, including a dramatic decrease in the local photoelectric absorption of soft X-rays, a decrease in the strength of the Fe and possibly of the Si K fluorescence features, underpredicted lines in two ions each of Ne and N (suggesting abundances that are ~1.5–3× and ~4× solar, respectively), and broadening of the strong Ne X Lyα and O VIII Lyα lines. In addition, we note certain traits in the γ Cas spectrum that are different from those of the fairly well studied analog HD 110432 – in this sense the stars have different "personalities." In particular, for γ Cas the hot X-ray component remains nearly constant in temperature, and the photoelectric absorption of the X-ray plasmas can change dramatically. As found by previous investigators of γ Cas, changes in flux, whether occurring slowly or in rapidly evolving flares, are only seldomly accompanied by variations in hardness. Moreover, the light curve can show a "periodicity" that is due to the presence of flux minima that recur semiregularly over a few hours, and which can appear again at different epochs.

Key words. stars: emission-line, Be – stars: individual: γ Cas – X-rays: stars

1. Introduction

The observed properties of γ Cas (B0.5 Ve; $m_V = 2.25$) in ultraviolet to infrared wavelengths have led to major discoveries related to the Be-phenomenon since its discovery as the first of what became known as "Be stars" (Secchi 1867). However, its X-ray emission is not typical of this kind of object (White et al. 1982). The X-ray emission of γ Cas is dominated by a hot plasma component ($kT \sim 10$–12 keV), with mildly high luminosity ($\sim 10^{32-33}$ erg s^{-1}) and variable flux (Smith et al. 2004, and references therein). Be stars at large are softer X-ray emitters ($kT \sim 0.5$ keV) with lower luminosity ($\lesssim 10^{32}$ erg s^{-1}) and little variability (e.g., Berghöfer et al. 1997). In contrast, most of the well investigated Be/X-ray binary systems are Be+neutron star systems and show a high luminosity ($\gtrsim 10^{33}$ erg s^{-1}) and a distinctly nonthermal high energy distribution. Notably, no large X-ray outburst has been observed in γ Cas. This is at variance with the behavior witnessed in many classical Be/X-ray systems. γ Cas is now known to be in a 204-day binary, with an eccentricity variously determined to be near $e = 0$ and 0.26 (Harmanec et al. 2000; Miroshnichenko et al. 2002). Little is known about the secondary, except that it is likely to have a mass in the range 0.5–2 $M_\odot$. Recently, X-ray properties similar to those of γ Cas have been observed in a small but growing number of Be stars: the γ Cas-like stars (Motch et al. 2007; Lopes de Oliveira et al. 2006; Lopes de Oliveira 2007).

A conclusive explanation for the X-ray emission of γ Cas and its analogs is lacking. The first suggestion to explain the hard X-ray emission of γ Cas was that it is powered by accretion of matter from the Be wind or disk onto an accreting neutron star (White et al. 1982). More recently, some have advocated the presence of an accreting white dwarf companion. This suggestion comes from several X-ray characteristics of cataclysmic variable systems (e.g., Murakami et al. 1986; Kubo et al. 1998), such as their thermal nature and only moderate X-ray luminosity. However, the analogy is incomplete upon further scrutiny, and X-rays would have to come from accretion onto a white dwarf representative of a new class of Be/X-ray binaries (Lopes de Oliveira et al. 2007) and have a high efficiency of mass accretion energy to X-ray flux.

A second proposed scenario suggests that the X-ray emission of γ Cas is a consequence of magnetic interaction between its stellar surface and a Be (Keplerian decretion) circumstellar disk that entrains a magnetic field. This idea is based in part on the correlations of the UV and optical variabilities with the X-ray light curve and also indirect evidence of magnetic field observed in this star. This evidence takes the form of migrating subfeatures running blue-to-red through optical and UV line profiles (Yang et al. 1988; Smith et al. 1998b) and also the discovery of

* This work is based on observations obtained with XMM-*Newton*, an ESA science mission with instruments and contributions directly funded by ESA Member States and NASA.

a gray, robust, 1.21581-day feature in the star's light curve. This periodicity must be very near or identical to the star's rotation period (Smith et al. 2006). The inference of a disk connection is based on the cyclical aspect and reddish tinge of the optical cycles that correlate with the X-ray ones. It is also supported by patterns of variability in the C IV and Si IV lines that are occasionally seen in the X-ray light curve (Cranmer et al. 2000). One piece of evidence for this interaction comes from the observation of highly redshifted *absorption* UV lines, suggestive of material being ejected from the circumstellar environment toward the star with enough energies to produce ~10 keV X-rays when they impact the star (Smith & Robinson 1999).

Both the magnetic disk and accretion interpretations have important astrophysical implications. The former suggests that disk dynamos operate and also that these stars are possible protomagnetars. The accretion interpretation would imply the presence of a neutron star in an unusual accretion regime, or a white dwarf with novel properties. The presence of a white dwarf is still speculative, but such objects are predicted to be common as secondaries in models of evolution of binaries with B primaries. The resolution of the mystery of the production of X-rays in "γ Cas stars" could lead to a breakthrough in either of these fields.

We have focused our efforts to try to understand the origin of the X-rays of γ Cas and analog Be stars. In this paper we confine ourselves to the X-ray properties of γ Cas from high and medium resolution spectroscopy and timing studies using data obtained by XMM-*Newton* satellite. *Chandra* HETG data are also reinvestigated.

2. Previous X-ray observations of γ Cas

Several *Rossi X-ray Timing Explorer (RXTE)* observations of the light curve of γ Cas detailed by Smith et al. (1998a) and Robinson & Smith (2000) (hereafter "SRC98" and "RS00", respectively) have disclosed that the light curve undergoes variations on rapid (flaring), intermediate (several hours) and long (2–3 month cycles) timescales. We summarize the flaring results first as follows:

- flares (shots) are ubiquitous, except during brief periods of very low X-ray flux. The reoccurrence of these lulls is often cyclical;
- individual flare profiles are narrow and symmetrical in shape;
- collectively flares show a log-normal distribution in energy;
- the flares show an approximately $1/f$ distribution down to the photon limit of the instrument (for *RXTE* about 4 s). Occasional groups of flares (aggregates) last as long as a few minutes, and indicate the end of this red noise dependence.
- spectrophotometry of shots indicates that their flux is usually difficult to distinguish from that of the underlying basal flux. That is, the two components have about the same high temperature of 10–12 keV.

Apparently random variations of several hours and 10's of percent amplitude occur often in the γ Cas X-ray light curve. One long simultaneous observation with the *Goddard High Resolution Spectrograph* (GHRS) on the *Hubble Space Telescope* established the correlation of small-amplitude UV continuum fluctuations (Smith et al. 1998a; Smith & Robinson 1999) and the concomitant absorptions in either lines arising from either lower or higher than expected ionization and excitation states (SR99).

Long-term variations have also been reported with cycle lengths of 50–91 days and amplitudes of a factor of three (Robinson et al. 2002, "RSH02"). These are so far well correlated with corresponding cycles in optical bands (Johnson *B* and *V*). Although the optical amplitudes are 100 times smaller than the X-ray ones they are still much larger than in terms of luminosity output and therefore cannot be the result of reprocessing of X-rays. Rather, a common mechanism appears to mediate both variabilities.

Modulations with several hours timescales were suggested by previous X-ray satellites. Frontera et al. (1987) reported a modulation with timescale of ~1.67 h from EXOSAT observation on 1984 December 7, while Parmar et al. (1993) argued from a reanalysis of this data that such an oscillation arise from statistical fluctuations in the red noise spectrum of the source. Also, Parmar et al. (1993) have not found periodic oscillation in other EXOSAT data obtained on 1984 December 25–26. A ~2.3 h oscillation was suspected by Haberl (1995) from ROSAT observation on 1993 July 16–17. Owens et al. (1999) found weak evidence for a ~0.6 h and 2.6 h in BeppoSAX observation of γ Cas carried out on 1998 July 20-21. None of these suspected detections could be found by subsequent monitorings of the star with the RXTE (e.g., Smith et al. 2000).

Pre-high resolution spectroscopy of γ Cas has demonstrated that its X-ray emission is dominated by a thermal component with $kT \sim$ 10–12 keV (Murakami et al. 1986; Parmar et al. 1993; Kubo et al. 1998; Owens et al. 1999). These spectra exhibited Fe XXV and Fe XXVI Lyα K line strengths consistent with this temperature, but they are consistent only with a subsolar Fe abundance of 0.2–0.4 $Z_\odot$.

Prior to this paper, the only high dispersion spectrum of γ Cas was obtained on 2001 August 10 by the *Chandra* High Energy Transmission Grating (HTEG) discussed by Smith et al. (2004) (hereafter "S04"). This spectrum showed a complex structure caused by plasma radiating in at least 3–4 temperatures ranging from about 12 keV to about 0.15 keV. The hot component in turn consisted of two subcomponents with very different ($\sim 10^{23}$ cm^{-2} and 3×10^{21} cm^{-2}) column densities. While the Fe K lines again indicated abundances of only $0.22 \pm 0.05\, Z_\odot$ other Fe lines arising from the L-shell give abundances which were consistent with the solar value. The strengths of other lines were also consistent with solar abundances.

3. Observations and data reduction

γ Cas was observed by the XMM-*Newton* X-ray observatory on 2004 February 5 during about 68 ks in the revolution 762 (ObsId 0201220101). This observation was performed with the EPIC *pn* camera running in the *fast timing mode* (timing resolution of 0.03 ms), connected to the *thick* optical filter, and with the high spectral resolution RGS1 and RGS2 cameras. The optical monitor was blocked as usual for bright optical sources, and the central CCDs in the MOS1/2 cameras were switched off in order to avoid overloading the telemetry. Data reduction has been made using the Science Analysis System (SAS) software v8.0.1. All data were reprocessed using the pipeline EPPROC (for EPIC *pn* camera) and RGSPROC (for RGS cameras) tasks. For the timing analysis, we use the Z_n^2 Rayleigh (Buccheri et al. 1983) and the Scargle/Midas (Scargle 1982) peridograms, and the Xronos[1] package. For spectral fits, the XSPEC[2]

[1] http://heasarc.nasa.gov/docs/xanadu/xronos/xronos.html

[2] http://heasarc.nasa.gov/docs/xanadu/xspec/index.html

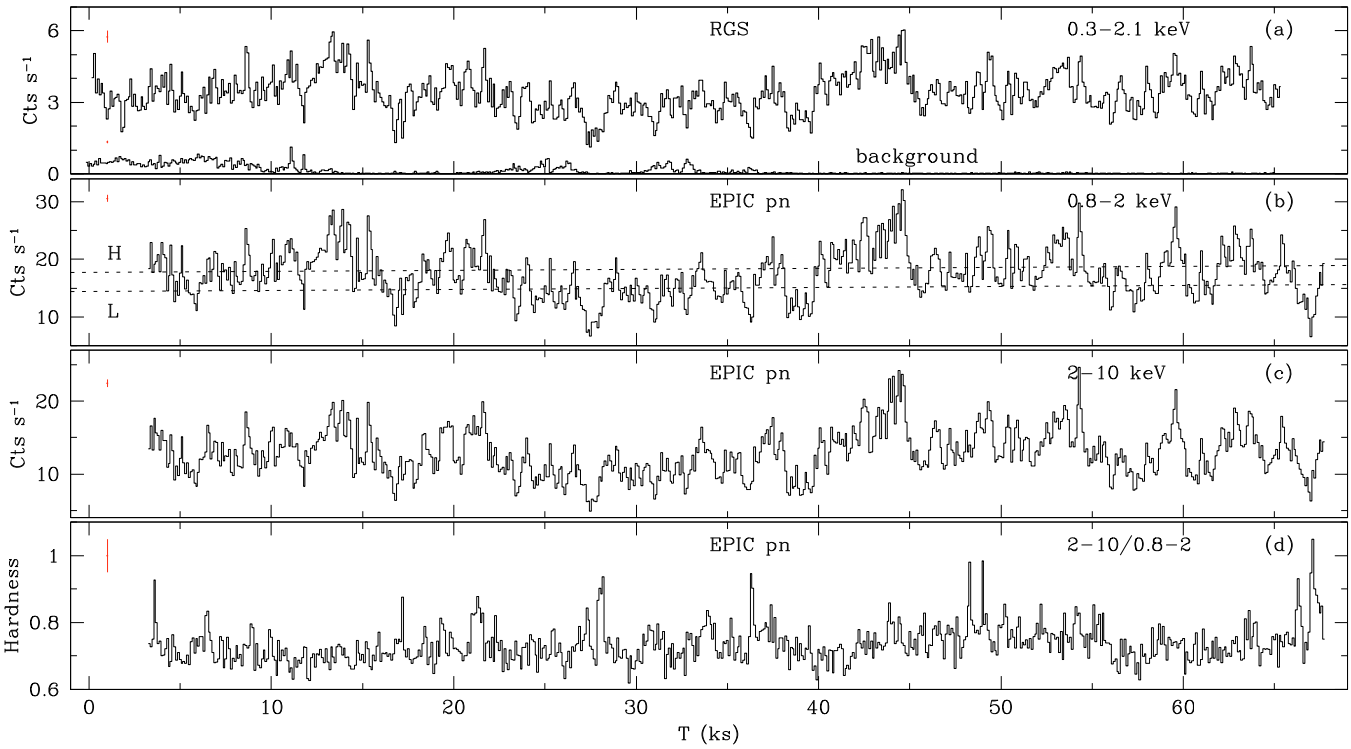

Fig. 1. a) RGS1+RGS2 light curve combining 1st and 2nd orders and the RGS1 background light curve, and EPIC *pn* light curves in the **b)** 0.8–2 keV and **c)** 2–10 keV X-ray bands, and the respective **d)** hardness ratio. Time bins of 100 s. Upper limits for error bars at 1σ are plotted in the left corner of the figures. The horizontal lines in panel **b)** represent the thresholds adopted to define the high (H) and low (L) state spectra (see Sect. 5.5).

software v11.3.2 was applied. The EPIC *pn* data obtained in the fast timing mode have a doubtful calibration and increased noise especially at softer energies (<0.5 keV; Guainazzi 2008) and, to be on the safe side, timing analysis was restricted to broad-bands at the 0.8–10 keV energy range without relevant loss of informations. For spectral studies, since we have high quality spectra from RGS1 and RGS2 cameras covering the soft X-rays (6.2–38 Å; or ~0.3–2 keV), we use the EPIC *pn* data as complementary data covering the hard part of the spectrum (1.25–4.1 Å; or ~3–10 keV). We noticed that the inclusion of the low energy part of the EPIC *pn* data produces systematic residuals that can be connected to calibration uncertainties. Because of the high count rate of γ Cas, the inclusion of times with slight background flares during the XMM-*Newton* observation has little impact on its EPIC *pn* and RGS light curves. However, we opted for excluding these times in the spectral analysis. The resulting exposure times in the flare-free good time intervals were 48 ks for the RGS1 and RGS2 cameras and 51.2 ks for EPIC *pn*.

We reinvestigated the *Chandra* data of γ Cas obtained on 2001 August 10 with the HETG during about 52 ks (ObsID 1895) with the CIAOv4.0, reported by Smith et al. (2004). Our purpose was to compare the *Chandra* and XMM-*Newton* spectra of γ Cas from the same analysis techniques and thus to insure that any differences between the derived parameters are not due to the model fitting programs. Our reanalysis of the *Chandra* spectrum with XSPEC and families of *mekal* models gives results consistent with those reported by S04, obtained from Sherpa and APEC models.

4. Timing studies

The soft (0.8–2 keV) and hard (2–10 keV) light curves of γ Cas are marked for strong variabilities on timescales ranging from a few to thousand of seconds (Fig. 1). On long timescales the variation attains ~80% of the mean flux. Superposed on this global modulation are ubiquitous flare-like events. We note in particular that the soft X-ray light curve responds faithfully to the rapid flares of the high energy light curve. In addition, the hardness of the source (Fig. 1c) usually exhibits nearly the same variations as the integrated flux. For example, the formal slope of the hardness-total count rate curve from our observations (not shown) is only $(5.2 \pm 2.9) \times 10^{-4}$.

These findings are similar to those reported by SRC98, though RS00 found that shot fluxes tended to exhibit a lower (softer) ratio.

Figure 2a exhibits the power spectrum of the EPIC *pn* events from the combined spectral bands shown in Fig. 1. A key point from this figure is that at frequencies above about 0.003 Hz the slope of the distribution is significantly steeper than –1. This was also noted by SRC98 and RS00, who found slopes of –1.23 and –1.36 in 1996 and 1998, respectively. The difference between those values was already marginally statistically significant, and the current result is certainly even more significantly different from the 1996 result. As noted by RS00, the difference between these slopes and –1 is most likely due to a relative prevalence of strong, longer-lived flares as compared to rapid short ones in these data. RS00 reported $1/f$ slopes in their 1998 light curves that were intermediate between the 1996 slope of –1 and the present steeper one. The explanation for the knee at about 0.003 Hz is again likely to be caused by the absence of discrete flares with timescales longer than a few minutes.

The break is due to the dominance of apparently random variations that often occur in the X-ray light curve on timescales of about a half hour or longer. At least some of these appear to be connected with variations in the UV continuum, which Smith et al. (1998a) have associated with the partial

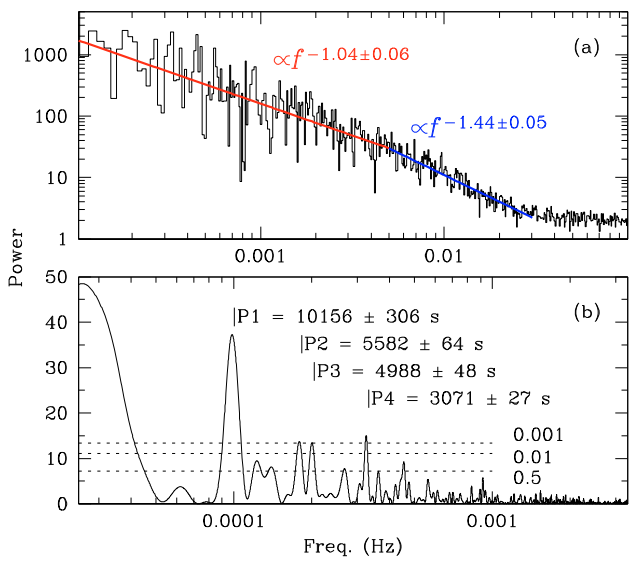

Fig. 2. Power spectrum. *Top*: from EPIC *pn* events at 0.8–10 keV, rebinned as a geometrical series. Bottom: from 0.8–10 keV EPIC *pn* data binned to 100 s; the dashed lines represent the confidence levels.

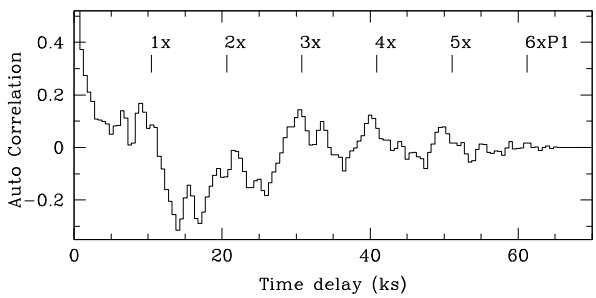

Fig. 3. Autocorrelation from 0.8–10 keV light curve binned to 500 s. P1 refers to result of Fig. 2b.

occultation of the star by rotationally advected translucent corotating clouds.

Another interesting feature emerging from the autocorrelation analysis of a light curve obtained by the RXTE satellite (Fig. 3) was the reappearance of periodic flux lulls. Following the procedure of Robinson & Smith (2000) we have cross-correlated both the fluxes in our XMM-*Newton* light curve and also the reciprocals of these fluxes. The latter exercise was carried out because RS00 had found that the autocorrelation of the direct fluxes produced no distinguishable features, whereas the autocorrelation of the reciprocal fluxes produced dramatic variations with lags of spacing of 7.5 h and higher multiples. These authors reasoned that this different behavior could come about if X-ray active centers at various latitudes of the rotating star would not produce marked features in the autocorrelation curve. However, features would be observed from the curve generated from the reciprocal fluxes if only a few longitudes of the star were not covered with X-ray activity. Our results, shown in Fig. 3 for the direct flux, produced rather similar curves for both the direct and reciprocal fluxes, indicating that the distribution of X-ray centers had rearranged themselves dramatically between the two epochs of observation. The curve itself shows evenly spaced maxima every ~10 156 s (2.8 h; Fig. 2b). On a subsequent study of six *RXTE* light curves of γ Cas, Robinson et al. (2002) discovered that autocorrelation peaks were most apparent in light curves associated with flare fluxes. These authors found that the features are centered at different time lags at different epochs, and occasionally did not occur at all. At various times these authors found spacings at 7.5 h, 3.5 h, and 5.8 h. The 2.8 h spacing we now find appear to be a recurrence of the same cycle length these authors found during a long RXTE observation in 2000 December. As Robinson et al. (2002) found, the autocorrelation peaks seem to be caused by an absence of flux (lulls) at different times. As such, they seem to hint at the existence of X-ray relaxation cycles in the γ Cas environment. In contrast, Lopes de Oliveira et al. (2007) found no such lulls in the light curve of HD 110432.

5. Spectroscopic properties

5.1. Comparison with previous Chandra HETGS spectrum

We have obtained a XMM-*Newton* spectrum in order to investigate time-dependent differences and also to exploit the higher effective aperture of the system, albeit with lower resolution at higher energies. The XMM-*Newton* provides coverage over longer wavelengths (~1–38 Å) than an *Chandra* spectrum with the high and medium energy gratings (~1.5–25 Å).

Our XMM-*Newton* spectrum shows the same general properties as the 2001 *Chandra* spectrum (Fig. 4). Both spectra show continua consistent with a multi-component thermal model that includes a number of Lyman α lines of hydrogen-like ions, helium-like ions, as well as a few Lyman β lines. Fluorescent lines from lower ion stages of Fe and Si are also visible. The high energies are dominated by the presence of the "Fe K complex" (Fe XXVI Lyα, Fe XXV, and fluorescent Fe K lines) in the range 1.7–2 Å. The two spectra of this aggregate look similar, except that the fluorescence feature is weaker in the XMM-*Newton* spectrum. However, our RGS spectrum reveals many more details than the *Chandra* one because of the XMM-*Newton*'s larger effective aperture as well as an extension to longer wavelengths and because in 2004 the soft X-rays of γ Cas were attenuated far less than in 2001. These circumstances allowed us to probe to lower temperatures and to better judge the number of components required to fit both lines and continua in the soft X-ray region.

5.2. Selection of multi-component modeling

Our models are the results of fitting both the continua and the line strengths in a multivariable solution with either the *mekal* formulation for optically thin plasmas, or a related model, *vmekal*, in which individual elemental abundances can be determined independently. A *Gaussian* line was included to describe the fluorescence feature arising from low-ion stages of Fe at 1.94 Å (6.4 keV), not incorporated in the *mekal* code. In all cases we adopted the *phabs* code to describe the photoelectric absorption. When required, we assumed the Hipparcos distance of 188 pc for γ Cas (Perryman 1997).

The high quality of our EPIC *pn* and RGS spectra allowed us to determine in detail the thermal components required to fit the line and continuum fluxes. This was especially important in allowing us to test whether the plasma has a continuous range of temperatures. Initial explorations showed that contributions from 3 or 4 temperatures are necessary. In addition, otherwise mediocre fits to the continua (especially the soft continuum) required us to consider a two-absorption column model. We found first the same hot temperature that many other investigators have reported. We will refer to this component as kT_Q.

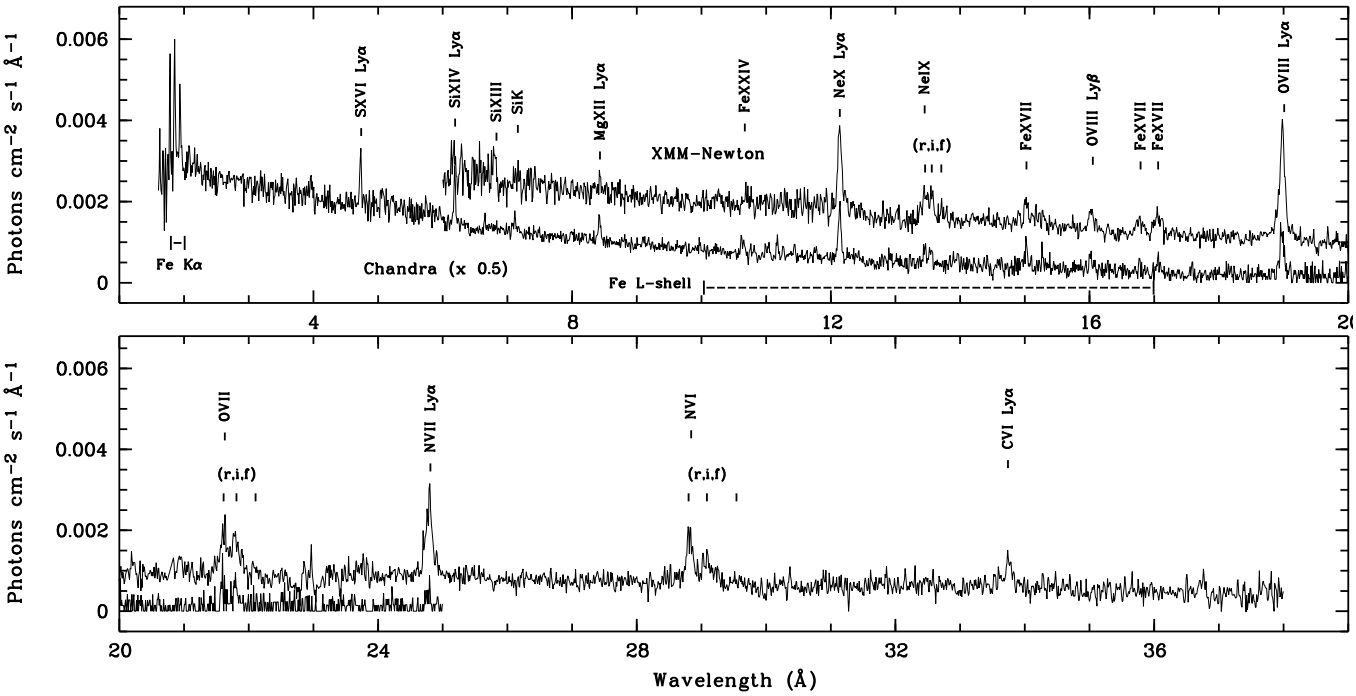

Fig. 4. The high resolution fluxed spectrum of γ Cas, from the RGS1+RGS2 XMM-*Newton* cameras combining 1st and 2nd orders, and from the HEG+MEG Chandra cameras combining all four first-order spectra.

This component has a 12 keV temperature and dominates the total X-ray flux. The carbon and nitrogen line spectra are emitted by a cool plasma with a temperature kT_1 of ~0.1 keV. The unabsorbed luminosity of this component, integrated over the range 0.2–12 keV, is ~6.8–8 × 10^{31} erg s^{-1}. One or two intermediate (warm) temperatures are likewise required to explain the presence of lines of oxygen, neon, magnesium, *silicon,* a few Fe ions with L-shell configurations (Fe XVII-XXIV), and the Fe XXV line (Figs. 4 and 5).

Before refining the initial 3 and 4 component models further, we attempted to determine whether these multiple thermal components were discrete or could be part of a continuous distribution, as might be expected in a single, thermally differentiated plasma. To continue tests using this initial set of simple models, we froze all but one temperature in our 4-T model and computed models for the remaining temperature specified over graduatedsteps. We made movies of these results overplotted with the observations and determined those values of the scanned temperature which allowed us to judge the best agreement with the observations. This technique also allowed us to note whether predicted lines are not observed as well as to test whether the principal plasma components are essentially monothermal. Figure 6 demonstrates this for kT_2 in M2 (4-T), which is necessarily confined within the range 0.5 and 1 keV. This plot shows the absence of Fe XXIII and strong Fe XXIV lines, as marked on our 10–13 Å segment of our RGS2 spectrum (RGS1 shows a gap at this wavelength). These lines would be stronger visible if the temperature were in the range 0.7–0.9 keV, and yet they are not seen. This fact eliminates the possibility that kT_2 is a distribution of temperatures extending to higher temperatures than 0.7 keV. On the lower bound our models predict the presence of the Fe XVIII 14.2 Å line for temperatures ≤0.5 keV, and this is not visible either. In addition, the abrupt disappearance of components from the O VII complex in the models shows that the absence of intermediate temperature plasma extends from 0.5 keV to about 0.2 keV. Altogether these

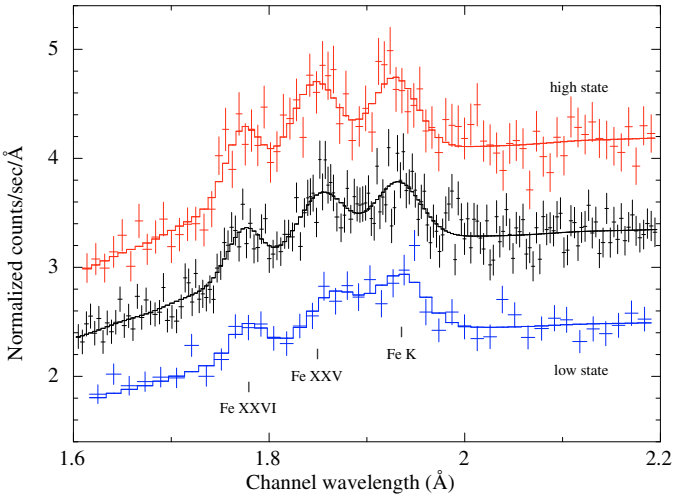

Fig. 5. The Fe Kα complex and its best fit determined from the model bremsstrahlung + 3 Gaussian lines for the low and high-state spectra (*bottom and top*, respectively) and the integrated spectrum. See details in Sect. 5.5.

diagnostics indicate that the kT_2 component in the γ Cas environment is limited to a very narrow range of temperatures centered near 0.6 keV and that it is distinct from a lower or higher plasma component. This statement can probably be extended to the spatial separation of the warm and cool plasmas as well.

Proceeding with this analysis, the weak Mg XII Ly α line hints the existence of a warm kT_3 component at ~2 keV, although some of our models have managed to achieve fits without it. The absence of yet other Fe L lines indicates that there is likely no plasma emission in the range of 2.5 to at least 5 keV. Also, the presence of the Fe XXVI Lyα feature, the main *line* diagnostic in the hard X-ray spectrum of γ Cas, requires a temperature of at least 8 keV. The Fe XXV Lyα line requires a value significantly

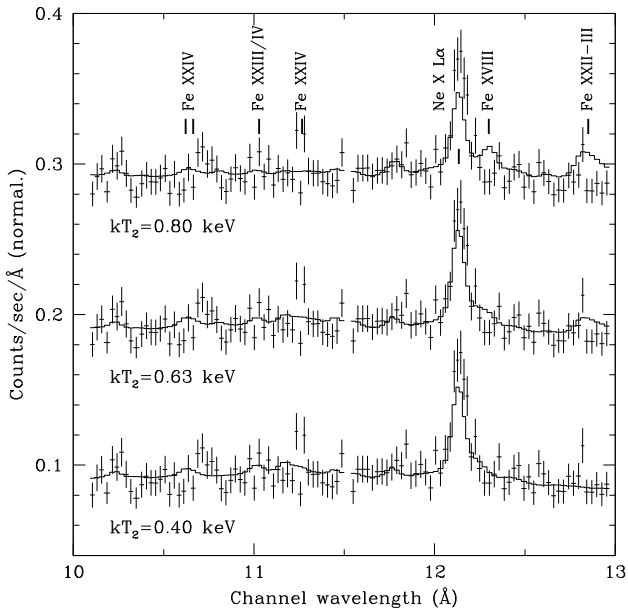

Fig. 6. The observed RGS2 spectrum in the 10–13 Å region for three trial values of kT_2 bracketing our model M2, in each case offset vertically for convenience. This figure depicts the Ne X Lyα and predicted positions of Fe lines arising from several ions, and the preferred temperature $kT = 0.63$ keV for kT_2. These predictions allow us to place limits on the lower limit to the range of the warm component, kT_2 (see text). The emission bump at 10.23 Å arises from Ne X Lyβ, and it is not fit in the range of temperatures shown.

lower than this limit, and this means that it cannot be formed in the kT_Q plasma component alone. In Fig. 6 a feature due to Ne X Lymanβ is present. This feature, visible in both the individual RGS1 and RGS2 spectra, cannot be easily fit with our thermal equilibrium (*mekal*) models.

It is quite possible that the kT_Q component consists of some distribution of temperatures around a mean value of 12–13 keV. This inference is supported by the occasional color variations in the high energy light curve of γ Cas (SRC98), suggesting the presence of hot many separated exploding gas volumes having a small range of temperatures.

The upshot of these considerations the presence and absence of various lines in this spectrum forces the conclusion that the plasma does not exhibit a continuous Differential Emission Measure (DEM). Rather, there are gaps over the ranges of about 2.5–8 keV, 0.7–1 keV, and 0.2–0.5 keV. S04 had suspected that a continuous DEM was inappropriate but could not state it conclusively because of the pronounced photoelectric absorption of the *Chandra* soft-energy spectrum.

5.3. Model fitting

The above procedures allowed us to refine our initial 3-T and 4-T models, utilizing both line and continuum flux information. Further attempts to search for a continuous Differential Emission Measure from the continuum alone, such as with a cooling flow *cemekl* led to significantly degraded fits even in the continuum[3].

[3] The *cemekl*/*cevmkl* code describes a multi-temperature plasma based on the *mekal* code, in which the emission measures of the plasma scale with their temperature as $(T/T_{\max})^{\alpha}$; $\alpha = 1$ corresponds to the adiabatic case.

The fits converged for $kT_{\max} \sim 42$ keV and $\chi^2_\nu = 2.4$. Freezing $kT_{\max}$ to 12 keV produced an unacceptably high $\chi^2_\nu = 6.4$. We next tried a composite model *cemekl* + *mekal*. This resulted in temperatures of $kT_{\max} \sim 12$ keV and $kT \sim 0.9$ keV for each component, respectively, and a $\chi^2_\nu = 1.75$. This model failed to describe the continuum at high energies and underpredicted the following features: the Fe XXV line in the Fe Kα complex, the Fe L-shell lines, OV III Lyβ, the *fir* triplet of O VII, N VII Lyα, and Ne X Lyα. Allowing the *cemekal* α parameter to vary did not improve the fits.

Table 1 shows the results of our analysis in terms of three basic models. Columns 2, 3, and 4 list the values determined for the temperature, column density, the modeled unattenuated flux, the resulting percentage of the total X-ray flux, and emission measures for the three and four component models, and the Fe abundance derived from the Fe XXV and Fe XXVI Lyα ions. In all cases the high temperature component we designate as kT_Q was found to lie near 12–14 keV. Column 2 of Table 1 shows the solution for a 3-T model, "(M1)", that includes a cool and warm components (kT_1 and kT_2, respectively) as well as the dominant one, kT_Q. The cool/warm component fluxes were attenuated by a column $N_{\mathrm{H_a}}$ while the hot one was attenuated by $N_{\mathrm{H_b}}$. Our 4-T model (Col. 3 of Table 1; "M2") gives the solution for the addition of a warm component having kT_3 and also attenuated by $N_{\mathrm{H_a}}$. The final column of the table, "(M3)", is the 3-T solution again. However, this time the hot component was attenuated by both $N_{\mathrm{H_a}}$ and $N_{\mathrm{H_b}}$ columns. In this model, the dominant hot subcomponent (kT_Q), affected by the individual $N_{\mathrm{H_b}}$ column, contributes to ~76% of the total flux. The second hot subcomponent (kT'_Q), warm (kT_2), and cool (kT_1) components were affected by a common $N_{\mathrm{H_a}}$ absorption column. Figures 7 and 8 show the unfolded spectrum for each model, allowing the reader to judge which of the various observed lines is formed in which plasma component. In our solutions we found that $N_{\mathrm{H_a}} \sim 2 \times 10^{21}$ cm^{-2} and $N_{\mathrm{H_b}} \sim 2$–3×10^{20} cm^{-2}. By comparison, the UV and Hα determined ISM column density to γ Cas from the literature is a scant 1–2 $\times 10^{20}$ cm^{-2}, which leaves only a little room for absorption of the soft X-rays within the source.

The 4-T fit we found included components kT_1, kT_2, kT_3, and kT_Q having values of about 14 keV, 2.4 keV, 0.6 keV, and 0.1 keV, respectively. For the 3-T models, the kT_3 component was omitted, but this omission must be compensated for in the Fe XXVI Lyα strength by decreasing the temperature from 14 to 12.5 keV.

It is worth noting that any of our models give us the desired $\chi^2_\nu \sim 1$. The residuals are mostly in the lines, not in the continuum, and the relatively high – although even acceptable – values of χ^2_ν (Table 1) are due in part to an inadequate description of the individual line profiles.

A key point to take away from the Table 1 is that although 84–90% of the total flux is radiated by the kT_Q (or kT_Q+kT'_Q) component(s), almost all the lines except for the Fe K complex is contributed by the cooler kT_{1-3}. The hot kT_Q component therefore provides no kinematic information. However, the possibility of multiple absorption columns and the presence of the fluorescence features of Fe and Si do provide potential geometrical descriptions for the emitting volumes.

Although S04's solution for the 2001 spectrum was similar in that it required a 4 thermal component fit, there were some small differences in detail that are significantly different. One of the clearest differences is with the precise temperature of a warm component (their "$kT_3 \sim 0.4$ keV cf. the $kT_2 \sim 0.6$ keV herein). A small increase in the O VIII/O VII Lyman α line

Table 1. Spectral fit results using the 3-T and 4-T models.

	Hot component, 1-col.		Hot component, 2-col.
	3-T (M1)	4-T (M2)	3-T (M3)
$N_{\rm H_a}$ (10^{22} cm^{-2})	$0.22^{+0.04}_{-0.03}$	$0.24^{+0.04}_{-0.04}$	$0.24^{+0.04}_{-0.04}$
kT_1 (keV)	$0.10^{+0.01}_{-0.01}$	$0.11^{+0.01}_{-0.01}$	$0.11^{+0.01}_{-0.01}$
$f_{\rm T_1}$ (erg cm^{-2} s^{-1})	$\sim 1.6\times10^{-11}$ (7.3%)	$\sim 1.9\times10^{-11}$ (8.4%)	$\sim 1.8\times10^{-11}$ (8.0%)
EM$_{\rm T_1}$ (10^{55} cm^{-3})	~0.5 (11.5%)	~0.7 (15.4%)	~0.6 (12.9%)
kT_2 (keV)	$0.64^{+0.03}_{-0.04}$	$0.64^{+0.03}_{-0.03}$	$0.62^{+0.03}_{-0.03}$
$f_{\rm T_2}$ (erg cm^{-2} s^{-1})	$\sim 4.0\times10^{-12}$ (1.8%)	$\sim 4.2\times10^{-12}$ (1.9%)	$\sim 4.0\times10^{-12}$ (1.8%)
EM$_{\rm T_2}$ (10^{55} cm^{-3})	~0.05 (1.1%)	~ 0.06 (1.3%)	~0.06 (1.3%)
kT_3 (keV)	...	$2.40^{+0.38}_{-0.26}$	...
$f_{\rm T_3}$ (erg cm^{-2} s^{-1})	...	$\sim 1.2\times10^{-11}$ (5.3%)	...
EM$_{\rm T_3}$ (10^{55} cm^{-3})	...	~0.2 (4.4%)	...
$kT_{Q'}$ (keV)	...	...	$12.38^{+0.30}_{-0.28}$ (*)
$f_{\rm T_{Q'}}$ (erg cm^{-2} s^{-1})	...	...	$\sim 3.2\times10^{-11}$ (14.3%)
EM$_{\rm T_{Q'}}$ (10^{55} cm^{-3})	...	...	~0.6 (12.9%)
$N_{\rm H_b}$ (10^{22} cm^{-2})	$0.029^{+0.002}_{-0.002}$	$0.022^{+0.002}_{-0.002}$	$0.019^{+0.003}_{-0.003}$
kT_Q (keV)	$12.55^{+0.31}_{-0.29}$	$14.32^{+0.59}_{-0.55}$	12.38 (*)
$f_{\rm T_Q}$ (erg cm^{-2} s^{-1})	$\sim 2.0\times10^{-10}$ (90.9%)	$\sim 1.9\times10^{-10}$ (84.4%)	$\sim 1.7\times10^{-10}$ (75.9%)
EM$_{\rm T_Q}$ (10^{55} cm^{-3})	~3.8 (87.4%)	~3.6 (78.9%)	~3.4 (72.9%)
$Z_{\rm T_{Q,Q'}}$ ($Z_\odot$)	$0.13^{+0.01}_{-0.01}$	$0.10^{+0.02}_{-0.02}$	$0.12^{+0.01}_{-0.01}$
Line (keV)	6.4^b	6.4^b	6.4^b
$\sigma_{\rm Line}$ (keV)	0.01	0.01	$0.09^{+0.04}_{-0.03}$
$f_{\rm tot}$ (erg cm^{-2} s^{-1})	$\sim 2.2\times10^{-10}$	$\sim 2.2\times10^{-10}$	$\sim 2.3\times10^{-10}$
EM$_{\rm tot}$ (10^{55} cm^{-3})	~4.4	~4.6	~4.7
χ^2_ν/d.o.f.^{a}	1.47/1532	1.44/1529	1.46/1530

Notes. Fluxes are given unabsorbed in the 0.2–12 keV energy band. In parentesis are the fluxes and EM in % of the total values. Plasmas with solar abundances, except for the [Fe] of the hot component. Quoted errors are at the 90% confidence level. Base model: $N_{\rm H_a}*(T_1+T_2+T_3+T_{Q'})+N_{\rm H_b}*(T_Q)$; see Sect. 5.3 for details.
$^{(a)}$ Degrees of freedom; $^{(b)}$ frozen parameter.

ratio for the XMM-*Newton* spectrum is indicative of the higher value we find. If a warm temperature is a quasi-permanent feature of the X-ray spectrum, it has definitely shifted from 0.4 keV to 0.6 keV between 2001 and 2004. The hot (~12–14 keV) and cool (~0.1 keV) component temperatures overlap. Although we cannot be sure if ~2 keV plasma existed in 2004, its possible presence is consistent with emission powered by a similar thermal component in the 2001 spectrum in their 2001 *Chandra* observation.

As already noted, one of most important differences from earlier results is that no high absorption column was needed to fit this spectrum. S04 found that the *Chandra* spectrum required a fitting with two hot plasma absorption columns. The first contributed 10–30% of the 12 keV component and was attenuated by an high absorption column of 10^{23} cm^{-2}. The second component, which is the dominant flux contributor to the observed spectrum at high energies, was attenuated by a column of $\sim 3\times10^{21}$ cm^{-2}. In contrast, most of the X-ray flux observed by XMM-*Newton* is affected by one dominant absorption column equivalent to $N_{\rm H}\sim 2$–3×10^{20} cm^{-2}, as derived from our 3-T and 4-T model with a single absorption column. However, for our models we were only able to fit the continua of our *combined* EPIC *pn* and RGS spectra with two absorption columns. Although the absorption of the $N_{\rm H_b}$ column, at $\sim$2–3 $\times 10^{20}$ cm^{-2}, is very low, it has much influence because it affects most (62–96%) of the total emission (see Table 1). The other absorption column has only a minor influence in absorbing the flux even though it is higher by a factor of 7–10 ($N_{\rm H_a}\sim 2\times10^{21}$ cm^{-2}). We note that the temperatures derived for each component in the models with one, as opposed to two, absorption columns are consistent with one another. The two column model also improved the descriptions of the lines formed at low energies, such as Ne X Lyα, and O VIII Lyα. The improvement of the fit with the second column over a model with a single column is supported by the F-test statistic, stating with a probability of only 4.7×10^{-5} that the derived decrease in χ^2_ν associated with the second column column is due to chance. The important conclusion from this is that the absence of a high absorption column as derived from the XMM-*Newton* observation suggests a dramatic rearrangement of cold circumstellar gas in the vicinity of the X-ray sources between 2001 August and 2004 February. Contrary to what is arguable for the 2001 epoch, it cannot be said that in 2004 the circumstellar disk was in front of a significant fraction of the soft X-ray source(s).

In order to estimate the origin of the long-wavelength lines in our models, we constructed a lineless continuum by excluding of the spectral regions lines in the 10–17 Å range and fit the resulting pure continuum spectrum to a bremsstrahlung

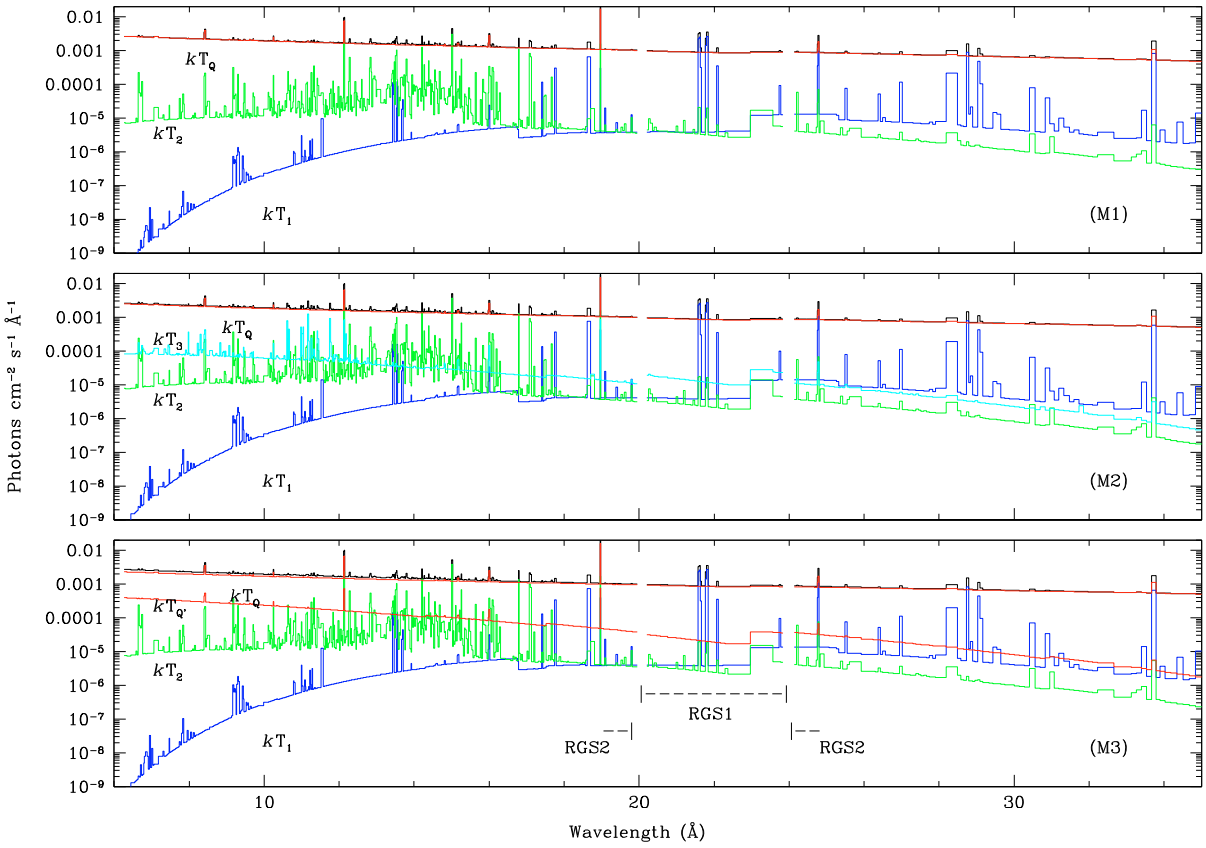

Fig. 7. Unfolded spectrum from RGS1 and RGS2 for each model in Table 1. The blue, green, cyan (light blue) and red lines correspond to the kT_1, kT_2, kT_3 and kT_Q (and $kT_{Q'}$), respectively, while the black lines correspond to the composite model.

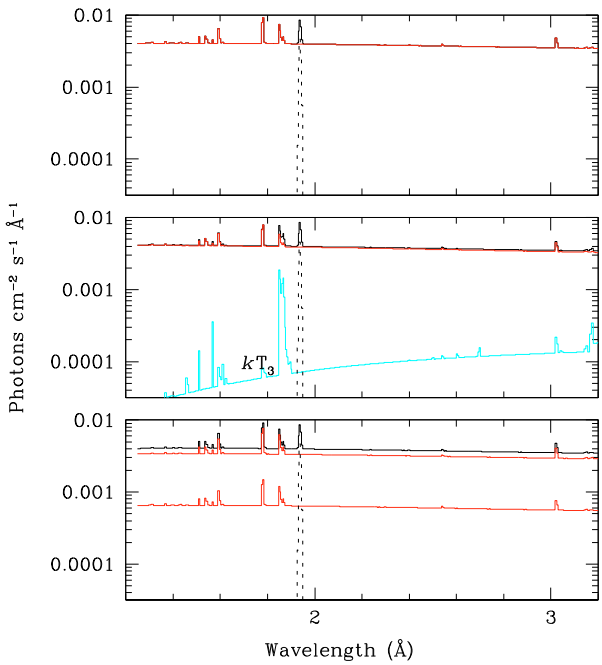

Fig. 8. Unfolded spectrum from EPIC *pn*, centered at the Fe Kα complex for each model in Table 1 (see Fig. 7 for details). The dotted lines refer to the *Gaussian* line at 1.94 Å (6.4 keV).

model. This model gave a value a slightly hotter temperature 13.2 keV for our hot component with a χ^2_ν of 1.17. The addition of a second bremsstrahlung component did not improve the fits ($kT \sim 0.04$ keV; χ^2_ν of 1.17). This result suggests that the determination of the low component temperatures, kT_1 and kT_2, is strongly driven by the lines alone.

Although all of our discussion has taken place in the context of equilibrium models, we agree with Smith et al. (2004), who suggested that the warm and/or cool plasma components could also result from nonequilibrium ionization processes, e.g. from the sudden impact of gas parcels ejected by flares into a dense stationary medium such as the Be disk. We suspect this could also be the reason why we observe Lymanβ transitions, such as the Lyβ transitions of Ne X and O VIII, that are not easily fit with equilibrium *mekal* models. A similar explanation might be also important in understanding the Fe XXVI Lyβ line at 8.3 keV of HD 110432, reported by Lopes de Oliveira et al. (2007), and which could not be fit with standard models for the ranges of temperature considered for this feature. The strong Lymanβ features hint at excitation temperatures in these plasmas that are higher than the ionization temperatures we found in Table 1.

5.4. Abundances and anomalous line strengths

For the most part the line strengths are consistent with solar abundances in our 3-T and 4-T models. The first and most conspicuous exception to this general result is the finding from Table 1 that the Fe abundance from K-electron Fe ions is $0.12 \pm 0.02\,Z_\odot$. This is a factor of two lower than any other studies in the literature (the S04 result was $0.24 \pm 0.02\,Z_\odot$). Because K-shell ion abundances of $0.1\,Z_\odot$ and $0.24\,Z_\odot$ are significantly different from one another, our result clarifies in a new way that

the Fe abundance derived from K-shell ions changes with time. Thus, the K-shell result may not reflect a global elemental abundance.

As also found by S04, the Fe abundance from L-shell ions is significantly higher than the Fe abundance from K-shell ions. We pursued the investigation of the Fe abundance from the Fe L-shell lines with the models M1, M2 and M3. In a new set of models we fixed other variables and solved for the Fe abundance of the soft temperature components kT_1 and kT_2. Our models suggest that the Fe L-shell abundance could be 0.4 to 1.3 $\times$ $Z_\odot$. This exercise verifies the distinctness of the Fe abundance arising from the L-shell lines on one hand and the K-shell lines on the other. For completeness note that a similar K- and L-shell Fe anomaly was reported by Lopes de Oliveira et al. (2007) for HD 110432.

The second apparent departure from solar abundances comes from the enhanced strengths of the lines of hydrogen and helium-like ions of neon and nitrogen. The formal abundances we find from our models are $Z_{\rm N} = 3.96^{+0.87}_{-0.69} \times Z_{\rm N,\odot}$ and $Z_{\rm Ne} = 2.63^{+0.27}_{-0.28} \times Z_{\rm Ne,\odot}$, assuming solar abundance for the other metals in the softest plasma and allowing for line broadening and bulk velocities. However, the allowed range of Ne abundances depends on the number and nature of the parameters left free in the fit, the most important being the assumed Fe L-shell abundance and the line broadening velocity. The hottest component dominates the NeX line flux with a smaller (~1/3) contribution from the T_2 thermal component. For instance, using bvapec instead of mekal and leaving Fe L-shell abundance free yields slightly lower abundances with $Z_{\rm Ne} = 1.65^{+0.38}_{-0.29} \times Z_{\rm Ne,\odot}$ and $Z_{\rm FeL-shell} = 0.41^{+0.18}_{-0.11} \times Z_{\rm Fe,\odot}$. This effect is due to the presence of a FeL-shell forest around the NeX Lα line and to the fact that the continuum level depends on the description of the FeL-shell lines. Although the limits for the abundances are not well determined, there is a clear excess above the solar values for N and Ne. The NeX line peak velocity is in the range of –110 to +230 km s^{-1} and displays a broadening velocity comparable to that of other bright emission lines.

A similar analysis was applied to the Chandra spectrum in order to determine whether the Ne enhancement was present or not in 2001 – it is not possible to expand the investigation to N abundance due to the low SNR of the NVII Lα line. The non-velocity broadened *mekal* model yields $Z_{\rm Ne} = 0.75 \pm 0.19 \times Z_{\rm Ne,\odot}$ consistent with the value obtained by Smith et al. (2004). However, since the observed NeX line apppears significantly wider than modeled, we used the *bvapec* model to take into account such a broadening. The larger NeX EW impacts the determination of the abundance yielding $Z_{\rm Ne} = 1.52^{+0.24}_{-0.24} \times Z_{\rm Ne,\odot}$ (or $Z_{\rm Ne} = 1.20^{+0.28}_{-0.24} \times Z_{\rm Ne,\odot}$ if the oxygen and iron L-shell abundances are left free, in which case we obtain $Z_{\rm FeL-shell} = 0.46^{+0.09}_{-0.09} \times Z_{\rm Fe,\odot}$). The broadened line profile fits the observed Ne line much better, with peak velocities then in the range of –60 to 260 km s^{-1} and broadening velocities of ~500 ± 200 km s^{-1}. These values are consistent with those derived from the RGS spectrum.

We note carefully that whereas the fluxes in these lines scale linearly with abundance, the equivalent widths, as formally defined with respect to the neighboring continuum flux, scale far more slowly because of the contribution to the local bound-free opacities from ions in a N-Ne rich plasma. Thus, we found an increase of only 35% with respect to the equivalent width measured in the *Chandra* spectrum. Our models with XSPEC validate this mild increase in equivalent width with abundance in detail. Given this reality, we anticipate that the true abundance errors are larger than those XSPEC computes based on photon statistics. Nonetheless, the anomalous excess cannot be discounted. Moreover, the possibility that the X-ray environment could be nitrogen-rich by a factor of 3–4 is unremarkable because enhancements are already a hallmark of massive stars evolving off the main sequence, although the reasons for this are still under discussion (Hunter et al. 2008). However, the apparent neon enhancement is of much greater interest because in a stellar evolution context neon is produced by carbon burning shortly before supernova detonation or in the interiors of some white dwarfs, and dredging to the surface of such elements is possible by various mixing processes.

Suggested alternatives to the straightforward abundance interpretation of the line strengths are the following: (i) instrumental artifact or a cosmic ray; (ii) an inappropriate temperature used in the modeling; and (iii) the line is strengthened by a microturbulent like broadening. Each of these possibilities may be dismissed in turn. (i) is unlikely because separate spectrum extractions from the positive and negative detector halves show consistent profiles. Likewise, we may rule out (ii) because a temperature of 0.6 keV is already ideal for Ne X formation, and a stronger feature cannot be produced given a standard abundance. Possiblity (iii) would require a large optical depth and strengthening of the line. However, even though the column density is probably high enough for photons to experience more than one mean free path through their transits across the medium, they are nonetheless scattered coherently. Therefore the line widths are unaltered by these histories. With these possibilities ruled out, we are forced to conclude that the neon and nitrogen abundances in the X-ray plasmas of γ Cas are high.

In considering the anomalous Fe abundance derived from Fe-K lines, but normal abundance from Fe-L lines in the γ Cas spectrum, S04 suggested that this could arise from an inverse FIP (first ionization potential) effect in the γ Cas environment that is similar to that found in the coronae of the Sun and other magnetically and X-ray active cool stars, such as AB Dor (Güdel et al. 2003). Although the details are still unclear, it appears that in a magnetic plasma low density environment differential ponderomotive forces, produced by wave heating and dependent on their first ionization potential, can prevent certain ions from migrating across a plasma and resulting in an altered measured chemical abundance (Laming 2004). Whether such a process is actually active in the environment of γ Cas, let alone whether it extends to Ne^{9+} ions, must be considered speculative. Its attractiveness lies in its potential to explain the different Fe abundances derived from K-shell and L-shell ions. Similarly, now in the framework of the accretion model, it is not clear, first, how Ne could be preferentially ejected from the white dwarf atmosphere or, second, how Ne could be enhanced without enhancing at the same time C, O, and Mg abundances.

5.5. The Fe Kα complex

In evaluating the equivalent widths (EW) of each emission iron line of the Fe K complex, we used the 5–10 keV photons acquired during low background phases of the XMM-*Newton* satellite's orbit. Our approach was to limit consideration of spectra accumulated only during low (L) and high (H) flux states observed in γ Cas (defined as the lowest and highest one-third fluxes of the total distribution in our light curve) and also during some 1000 time windows in which the detector background was low (see Fig. 1-b). Finally, we applied an absorbed bremsstrahlung model in order to describe the underlying continuum and three *Gaussian* lines to account the iron lines. Table 2

Table 2. Parameters of the emission lines of the Fe Kα complex from a bremsstrahlung + 3 Gaussian lines model.

	λ_C (Å)	EW (mÅ)	Flux[a] ($\times 10^{-5}$)
all observation:			
Fe K (fluorescence)	1.9312[60]	10[2]	$4.4^{+0.8}_{-1.0}$
Fe XXV	1.8533[55]	12[3]	$5.3^{+1.4}_{-0.9}$
Fe XXVI Lyα	1.7737[51]	7[2]	$3.1^{+0.7}_{-0.5}$
low state:			
Fe K (fluorescence)	1.937[12]	13[5]	$4.1^{+1.0}_{-1.7}$
Fe XXV	1.867[17]	12[4]	$4.1^{+1.5}_{-1.2}$
Fe XXVI Lyα	1.781[10]	7[3]	$2.2^{+0.9}_{-0.8}$
high state:			
Fe K (fluorescence)	1.9282[60]	10[3]	$5.6^{+1.0}_{-1.6}$
Fe XXV	1.8478[83]	13[4]	$7.6^{+2.2}_{-1.4}$
Fe XXVI Lyα	1.7737[76]	8[2]	$4.4^{+1.3}_{-0.9}$

Notes. Quoted errors are at 90% confidence level. The temperature of the bremsstrahlung model at 1.2–4.1 Å (3–10 keV) converges to kT = 13.36(+0.21/–0.25) keV.
[a] Total flux in line, in units of photons cm^{-2} s^{-1}.

Table 3. Parameters of the strongest emission lines.

	λ_C (Å)	EW (mÅ)	Flux[a] ($\times 10^{-4}$)	
Ne X Lyα^c	12.131[11]	125[18]	2.15[31]	(1.26 ± 0.16)
O VIII Lyβ^c	15.997[41]	40[14]	0.55[20]	(0.31 ± 0.16)
O VIII Lyα^c	18.9796[49]	360[28]	3.93[31]	(1.71 ± 0.26)
O VII r^b	21.60[90]	163[19]	1.72[20]	(0.77 ± 0.28)
O VII i^b	21.78[92]	149[19]	1.58[20]	(0.79 ± 0.40)
O VII f^b	22.097[d]	<32	<0.3	(0.13 ± 0.16)
N VII Lyα^c	24.79[99]	296[17]	2.76[16]	(0.61 ± 0.03)
N VI r^c	28.81[90]	<230	<2	...
N VI i^c	29.09[95]	<169	<1.4	...
N VI f^c	29.531[d]	<10	<0.08	...
C VI Lyα^d	33.736[64]	201[29]	1.37[20]	...

Notes. [a] Total flux in line, in units of photons cm^{-2} s^{-1}; in parenthesis are shown the values derived by Smith et al. (2004) from Chandra. [b] From RGS1. [c] From RGS2. [d] Frozen parameter. Quoted errors are at 90% confidence level.

and Fig. 5 show the results. The measured centroid energy of each modeled *Gaussian* line is, within the errors, in agreement with the theoretical values for the fluorescent, helium-, and hydrogen-like components of the Fe Kα complex. It is possible that there may be a slight inverse sensitivity of the fluorescence strength (relative to the Fe XXVI line), though this inference is of marginal statistical significance.

In our EPIC *pn* spectrum the strength of the fluorescence feature ($EW \sim -10$ mÅ) is weaker than when Chandra observed it ($EW \sim -19$ mÅ; Smith et al. 2004), in line with the fact that the attenuation of soft X-rays by cold matter is less. This suggests that the fluorescence emission feature is formed at least partially by the same medium that aborbs the soft-X ray flux.

Curiously, the analysis in the low and high-state spectra reveals that the FeK fluorescence feature may be marginally stronger in the low flux case. Although such investigation could not be expanded to a quantitative analysis of all spectral range because the relatively limited signal-to-noise in the final spectra for RGS1/2, we suspect that there is weak evidence for a weakening of the SiK feature for the low flux spectrum.

5.6. Helium-like diagnostics of electron densities

Our spectrum covers the regions of the He-like Ne IX, O VII and N VI complexes – but the N VI complex falls partially onto gaps in the CCD for RGS1 and RGS2. Each of these is comprised of a so-called fir (forbidden/intercombination/resonance) line triplet (see Fig. 4), and the ratio of their intensities can indicate whether the dominant excitation process for producing this triplet is collisional or photoionization. For example, if collisions are dominant, the ratio $G = (i + f)/r \sim 1$ obtains, whereas if photoionizations dominate the exitation $G \sim 4$ (e.g. Porquet & Dubau 2000; Porquet et al. 2001). From the O VII fir complex in our XMM-*Newton* spectrum, we estimate $G \sim 0.9 \pm 0.1$ for γ Cas. The N VI rif components are poorly measured because they fall within the gaps of the RGS2 detector. Nonetheless, by computing their ratios we find nearly the same value, $G \sim 0.7 \pm 0.3$. This suggests that the plasma is in the classical domain of collisional dominance. As it happens, the fir ratio alone cannot distinguish between quenching of the forbidden transition by collisions or by photoexcitations by a nearby strong UV source, such as the Be star.

5.7. Velocity broadening and shifts in warm plasma lines

In Table 3 we list the observed centroid wavelength, the equivalent width and the flux of lines for those lines for which meaningful measurements could be made. The best observed lines in the soft X-ray spectrum, Ne X Lyα and O VIII Lyα profiles are noticeably broadened. We evaluate the broadening of the lines by using the *bapec* model, a velocity- and thermally-broadened emission model from collisionally-ionized diffuse gas[4]. The *Gaussian* sigma for velocity broadening converges to ~400 km s^{-1} for a model like M1, M2 and M3 in Table 1, replacing the *mekal* by the *bapec* code. The line broadening was also measured on individual lines, not only on the whole spectrum. For example, we found a velocity broadening of 300 ± 70 km s^{-1} for the O VIII line. The RGS velocity is consistent with that reported by S04 (478 ± 50 km s^{-1}). We applied the same analysis to two RGS spectra of AB Dor acquired in 2000 and 2006 (obsID 0126130201 and 0160363001 with up-to-date calibration) and found in each case that the broadening of the O VIII line was less than about 70 km s^{-1} at the 90% confidence level, proving that the lines of γ Cas are indeed broadened.

In order to check for velocity shift in the lines, we run the models in Table 1 leaving the redshift parameter free. We found a overall redshift of ~200 km s^{-1} – and values for the parameters and χ^2_ν consistent with those shown in Table 1 – slightly larger than the typical error on the absolute wavelength scale of ~7 mÅ, or ~140 km s^{-1}.

5.8. Do our cool or warm plasma component arise in a radiative wind?

It has been believed for some time that X-ray emission in O and early B stars arises in sites associated with shocks distributed in the stars radiative winds (e.g. Leutenegger et al. 2006; Cohen 2008). Analyses of HETG spectra of other stars in the same general region of the H-R Diagram, for example of τ Sco (B0.2 V), β Cru (B0.5 III), and ζ Oph (O9.5 V) by Cohen (2003),

[4] http://cxc.harvard.edu/atomdb/

Cohen (2008), and Waldron (2005), respectively, paint a complex picture. The Cohen et al. analyses show that the winds of at least some early B stars cannot be described by a standard picture of wind-shocks, and indeed wind structures of at least τ Sco and ζ Oph may be influenced by the effects of channeling by magnetic fields in the regions surrounding the star. The temperatures of the gas are not yet known to vary but taken as a group range from about 3 to 25 MK. We note that the X-ray emission measures associated with winds in these stars have not been found to be variable so far.

γ Cas has such a wind, as evidenced by the profiles of doublets in UV resonance absorption lines of several ions, notably C IV, N V, and Si IV. These profiles exhibit Discrete Absorption features at 1000–1100 km s^{-1} and edge velocites of –1800 km s^{-1} (Doazan 1982; Kaper et al. 1996; Smith et al. 1998a,b). Our analysis shows the presence of soft X-ray components whose temperatures, fluxes, and emission measures (Table 1) are consistent with those of normal massive stars reported by Walborn et al. (2009), for example. It is thus expected that at least part of such emission is emanating from the radiatively driven wind of γ Cas. However, as can be seen in Fig. 7, the hottest component dominates also the soft part of the spectrum of γ Cas and the contribution of a pure radiative wind is overshadowed by this hot component. Establishing the presence of a luminosity change in the soft components supporting a non-wind origin is a complicated issue because of the presence of the Be disk itself (which may shield a part of the wind) and because the characteristics of the γ Cas' spectra in 2001 and 2004 are different from each other. It is worth noting that the X-ray 0.2–12 keV (unabsorbed) fluxes from the soft ($kT \sim 0.1$ keV) component in 2001 and 2004 are consistent with each other ($<1.7\times10^{-11}$ erg s^{-1} from Chandra and 1–2.7$\times10^{-11}$ erg s^{-1} from XMM-*Newton*), while the flux from the $kT \sim 0.6$ keV component has increased between 2001 and 2004 (from 0.7–2.2 to 2.5–6$\times10^{-12}$ erg s^{-1}). In conclusion, we cannot discard an additional contribution to the soft plasma in addition to that of a radiatively driven wind usually observed in massive stars.

6. Conclusions

We have reported the second high dispersion analysis of the X-ray spectrum of the X-ray anomalous B0.5e star γ Cas obtained by the XMM-*Newton* in 2004, and we find the following characteristics at this epoch:

a) the emission is due to an optically thin, thermal medium comprised of 3 to 4 discrete components but dominated by a hot component having $kT_Q \sim 12$–14 keV. The temperature of at least one component ($kT_2 \sim 0.6$ keV) has definitely shifted since the *Chandra* HTEG observation in 2001. It is possible that a $kT_3 \sim 2.4$ keV component exists too. If so it may represent plasma with nearly the same temperature found by S04. Further, the presence of a cool component with $kT_1 \sim 0.1$ keV is consistent with a value found by S04. This may or may not have the same cause as the wind-shocked fluxes emitted from other early B and Be stars. However, if so, it is a lower temperature than expected. Only part (at most) of the kT_2 plasma could be produced in the wind, and if so the large line widths evidenced in this component indicate a larger turbulent broadening than is typical of winds in other early B stars.

b) The hot kT_Q component appears stable and any distribution of temperatures of individual sites around this mean value must be small.

c) A subsolar abundance of iron is derived from the Fe XXV and Fe XXVI Lyα features, in agreement with several other determinations. As S04 also found, this Fe$_K$ abundance is significantly different of the abundance found from Fe-L ion lines. We have also discovered that [Fe$_K$] changes with time and was significantly higher in 2004.

d) The light curve of this star again shows ubiquitous, rapid flaring. This was also found by Lopes de Oliveira et al. (2007) in HD 110432. However, unlike HD 110432, color changes occurred only seldomly, and evidently not at all on the few hour timescale noted in HD 110432.

e) Our light curve shows a quasi-periodic lull every 2.8 h in 2004, similar to the cyclical lulls of 3.5 h, 7–7.5 h, and 5.8 h noted by RSH02. These appear to occur in most epochs.

f) A thick absorption column affected 25% of the hot component in August 2001, but it had disappeared by February 2004.

g) Apparently variable Fe K and perhaps Si K fluorescent features are present. These emissions correlate with an absorption column (point *f*) that attenuates soft X-rays.

h) Broadening of warm (kT_2) component lines was noticeable at both epochs but may have increased marginally from 2001 (~0.4 keV) to 2004 (~0.6 keV).

i) The strengths of lines of two ions each of N and Ne are underpredicted for XSPEC models with solar abundances. Upon consideration of alternative explanations, we have interpreted these as evidence of abundance enhancements. However, we do not understand the cause of these enhancements.

j) Given the identification of the Lymanβ feature in a few ions formed in the warm and cool plasmas, there is more than a hint of nonequilibrium processes in the environment of γ Cas. This suggests formation in an (at most) intermediate density environment, which is clearly separate from the very high density plasma in which the flares are formed (Smith et al. 1998a).

k) The unabsorbed flux of γ Cas at 0.2–12 keV in 2004 from XMM-*Newton* (~1.7–2.8 $\times$ 10^{-10} erg s^{-1}) is consistent with the value observed in 2001 from Chandra (~2–3.1 $\times$ 10^{-10} erg s^{-1}).

In several of these respects the X-ray behavior of γ Cas seems different from the one other analog studied in depth, HD 110432. In keeping with the differences of HD 110432, and indeed even the changing properties with time, we refer to this star as having "personality" – hence the title of this paper.

Several changes we have noted are as remarkable as they were unexpected. Most especially, we have noted changes in the geometry of the circumstellar environment as reflected in the disappearance of one of the two columns, and affecting ~25% of the hard emission. The strong attenuation of the 2001 soft X-ray spectrum was clearly evident. In addition, the strengths of the K fluorescence emission features decreased in line with the decrease of the column absorption, suggesting that the part of the emission is caused by scattering of hard photons through the attenuating column that was present at the earlier time.

The reduced attenuation of the soft X-rays partially accounts for the improved ability to study the nature of the warm and cool plasma emissions. As a result, it is finally clear that these components are almost monothermal and therefore are not part of an integral structure with a smoothly varying thermal emission measure, such as an accretion column or a cooling flow plasma. Moreover, the broadening of the lines has increased during the 2001–2004 interval, either because of an increase in a

quasi-turbulence or the splitting of a former single region into two with different projected radial velocities.

In contrast to the warm component, a study of the variations in the Fe K-shell lines with temperature shows that the hot plasma need not consist of a uniform kT_Q value. Rather, we believe that small variations in the hardness that are occasionally observed in our data and those discussed by SRC98, RS00, and RSH02 can be understood as variations of the instantaneous average temperature resulting from the rapid evolution of small number of flares and nearby basal emission regions.

The unique properties of each of the thermal components, the changing absorption column geometry, and increases in line broadening all provide new hints to the mechanism responsible for the X-ray production. Although on one hand, the disappearance of the strong absorption column and the lack of correlation between the fluorescence features no longer support the argument that the gas in the Be star's circumstellar disk strongly interact with the hard X-rays, the discreteness of the plasma components argues that they are likely to occupy distinct volumes.

Future generations of X-ray telescopes such as the International X-ray Observatory (IXO) will be important in refining our understanding of the spatial distribution of emission volumes of γ Cas and its analogs. Their observations promise to address such question as whether the observed line broadening can be tied to the rotational velocity of the Be star and to resolving distinct sources, such as corotating active regions.

Acknowledgements. R.L.O. acknowledges financial support from the Brazilian agency FAPESP (Fundação de Amparo à Pesquisa do Estado de São Paulo) through a Postdoctoral Research Fellow grant (number 2007/04710-1). We gratefully acknowledge the XMM-*Newton* User Support Group, in particular Nora Loiseau, Jan-Uwe Ness, and Matteo Guainazzi, for their help with problems on SASv8.0.1. We would like to thank the anonymous referee for his/her comments.

References

Berghöfer, T. W., Schmitt, J. H. M. M., Danner, R., & Cassinelli, J. P. 1997, A&A, 322, 167
Buccheri, R., Bennett, K., Bignami, G. F., et al. 1983, A&A, 128, 245
Cohen, D. H., de Messières, G. E., MacFarlane, J. J., et al. 2003, ApJ, 586, 495
Cohen, D. H., Kuhn, M. A., Gagne, M., et al. 2008, MNRAS, 386, 1855
Cranmer, S. R., Smith, M. A., & Robinson, R. D. 2000, ApJ, 537, 433
Doazan, V. 1982, in B Stars with and without Emission Lines, ed. A. Underhill & V. Doazan, NASA SP-456, 326
Ehle, M., de la Calle, I., Díaz Trigo, M., et al. 2008, XMM-*Newton* Users' Handbook, Issue 2.6, 15 July 2008
Frontera, F., Dal Fiume, D., Robba, N. R., et al. 1987, ApJ, 320, L127
Guainazzi, M. 2008, XMM-SOC-CAL-TN-0018, Issue 2.7.2 (4 November 2008)
Güdel, M., et al. 2003, ASP Conf. Ser., 277, 221
Haberl, F. 1995, A&A, 296, 685
Harmanec, P., Hadrava, P., Stefl, S., et al. 2000, A&A, 364, 85
Howk, J. C., Cassinelli, J. P., Bjorkman, J. E., et al. 2000, ApJ, 534, 348
Hunter, I., Brott, I., Lennon, D. J., et al. 2008, A&A, 676, L29
Kaper, L., Henrichs, H., Nichols, J. S., et al. 1996, A&AS, 116, 257
Kubo, S., Murakami, T., & Corbet, R. H. D. 1998, PASJ, 50, 417
Laming, J. M. 2004, ApJ, 614, 1063
Leutenegger, M. A., Paerels, F. B. S., Kahn, S. M., & Cohen, D. H. 2006, ApJ, 650, 1096
Lopes de Oliveira, R. 2007, Ph.D. Thesis, Universidade de São Paulo, Brazil, and Université Louis Pasteur Strasbourg I, France
Lopes de Oliveira, R., Motch, C., Haberl, F., Negueruela, I., & Janot-Pacheco, E. 2006, A&A, 454, 265
Lopes de Oliveira, R., Motch, C., Smith, M. A., Negueruela, I., Torrejón, J. M. 2007, A&A, 474, 983
Miroshnichenko, A. S., Bjorkman, K. S., & Krugov, V. D. 2002, PASP, 114, 1226
Motch, C., Lopes de Oliveira, R., Negueruela, I., Haberl, F., & Janot-Pacheco, E. 2007, in Active OB-Stars: Laboratories for Stellar and Circumstellar Physics, Proceedings of the conference held 29 August–2 September, 2005 at Hokkai-Gakuen University, Sapporo, Japan, ed. S. Stefl, S. P. Owocki, & A. T. Okazaki, San Francisco: Astronomical Society of the Pacific, ASP Conf. Ser., 361, 117
Murakami, T., Inoue, H., & Agrawal, P. C. 1986, ApJ, 310, L31
Owens, A., Oosterbroek, T., Parmar, A., Schultz, R., Stüwe, J. A., & Haberl, F. 1999, A&A, 348, 170
Parmar, A., Israel, G., Stella, L., & White, N. 1993, A&A, 275, 227
Perryman, M. A. C. 1997, The Hipparcos and Tycho Catalogues, ESA SP-1200
Porquet, D., & Dubau, J. 2000, A&AS, 143, 495
Porquet, D., Mewe, R., Dubau, J., Raassen, A. J. J., & Kaastra, J. S. 2001, A&A, 376, 1113
Prinja, R. K. 1989, MNRAS, 241, 721
Robinson, R. D., & Smith, M. A., 2000, ApJ, 540, 474 (RS00)
Robinson, R. D., Smith, M. A., & Henry, G. W. 2002, ApJ, 575, 435
Scargle, J. D. 1982, ApJ, 263, 835
Secchi, A. 1867, Astron. Nachr., 68, 63
Smith, M. A., & Robinson, R. D. 1999, ApJ, 517, 866
Smith, M. A., Robinson, R. D., & Corbet, R. H. D. 1998a, ApJ, 503, 877 (SRC98)
Smith, M. A., Robinson, R. D., & Hatzes, A. P. 1998b, ApJ, 507, 945
Smith, M. A., Cohen, D. H., Gu, M. F., et al. 2004, ApJ, 600, 972 (S04)
Smith, M. A., Henry, G. W., & Vishniac, E. 2006, ApJ, 647, 1375
Walborn, N. R., Nichols, J. S., & Waldron, W. L. 2009, ApJ, 703, 633
Waldron, W. L. 2005, ASPC, 337, 329
White, N. E., Swank, J. H., Holt, S. S., & Parmar, A. 1982, ApJ, 263, 277
Yang, S., Ninkov, Z., & Walker, G. A. H. 1988, PASP, 100, 233